Solid-State Electronics 136 (2017) 102–112

Contents lists available at ScienceDirect

Solid-State Electronics

journal homepage: www.elsevier.com/locate/sse

Hyperbolic metamaterials: Novel physics and applications

Igor I. Smolyaninov [a,*], Vera N. Smolyaninova [b]

[a] Department of Electrical and Computer Engineering, University of Maryland, USA
[b] Department of Physics, Astronomy, and Geosciences, Towson University, USA

ARTICLE INFO

Article history:
Available online 20 June 2017

The review of this paper was arranged by A. A. Iliadis, A. Akturk, R. P. Tompkins, and A. Zaslavsky

ABSTRACT

Hyperbolic metamaterials were originally introduced to overcome the diffraction limit of optical imaging. Soon thereafter it was realized that hyperbolic metamaterials demonstrate a number of novel phenomena resulting from the broadband singular behavior of their density of photonic states. These novel phenomena and applications include super resolution imaging, new stealth technologies, enhanced quantum-electrodynamic effects, thermal hyperconductivity, superconductivity, and interesting gravitation theory analogues. Here we briefly review typical material systems, which exhibit hyperbolic behavior and outline important novel applications of hyperbolic metamaterials. In particular, we will describe recent imaging experiments with plasmonic metamaterials and novel VCSEL geometries, in which the Bragg mirrors may be engineered in such a way that they exhibit hyperbolic metamaterial properties in the long wavelength infrared range, so that they may be used to efficiently remove excess heat from the laser cavity. We will also discuss potential applications of three-dimensional self-assembled photonic hypercrystals, which are based on cobalt ferrofluids in external magnetic field. This system bypasses 3D nanofabrication issues, which typically limit metamaterial applications. Photonic hypercrystals combine the most interesting features of hyperbolic metamaterials and photonic crystals.

1. Hyperbolic metamaterial geometries and basic properties

Hyperbolic metamaterials are extremely anisotropic uniaxial materials, which behave like a metal in one direction and like a dielectric in the orthogonal direction. Originally introduced to overcome the diffraction limit of optical imaging [1,2], hyperbolic metamaterials demonstrate a number of novel phenomena resulting from the broadband singular behavior of their density of photonic states [3], which range from super resolution imaging [2,4,5] to enhanced quantum-electrodynamic effects [6–8], new stealth technology [9], thermal hyperconductivity [10], high Tc superconductivity [11,12], and interesting gravitation theory analogues [3,13–17]. In the early days of metamaterial research it was believed that only artificially structured materials may exhibit hyperbolic properties. However, later on it was realized that quite a few natural materials may exhibit hyperbolic properties in some frequency ranges [11,18]. Moreover, even the physical vacuum may exhibit hyperbolic metamaterial properties if subjected to a very strong magnetic field [19].

Basic electromagnetic properties of hyperbolic metamaterials may be understood by considering a non-magnetic uniaxial anisotropic material with dielectric permittivities $\varepsilon_x = \varepsilon_y = \varepsilon_1$ and $\varepsilon_z = \varepsilon_2$. Any electromagnetic field propagating in this material may be expressed as a sum of ordinary and extraordinary contributions, each of these being a sum of an arbitrary number of plane waves polarized in the ordinary ($E_z = 0$) and extraordinary ($E_z \neq 0$) directions. Let us define a "scalar" extraordinary wave function as $\varphi = E_z$ so that the ordinary portion of the electromagnetic field does not contribute to φ. Maxwell equations in the frequency domain results in the following wave equation for φ_ω if ε_1 and ε_2 are kept constant inside the metamaterial [3]:

$$\frac{\omega^2}{c^2}\varphi_\omega = -\frac{\partial^2\varphi_\omega}{\varepsilon_1\partial z^2} - \frac{1}{\varepsilon_2}\left(\frac{\partial^2\varphi_\omega}{\partial x^2} + \frac{\partial^2\varphi_\omega}{\partial y^2}\right) \quad (1)$$

While in ordinary elliptic anisotropic media both ε_1 and ε_2 are positive, in hyperbolic metamaterials ε_1 and ε_2 have opposite signs. These metamaterials are typically composed of multilayer metal-dielectric or metal wire array structures, as shown in Fig. 1. The opposite signs of ε_1 and ε_2 lead to two important consequences. For extraordinary waves in a usual uniaxial dielectric metamaterial, the dispersion law

$$\frac{k_{xy}^2}{\varepsilon_2} + \frac{k_z^2}{\varepsilon_1} = \frac{\omega^2}{c^2} \quad (2)$$

describes an ellipsoid in the wave momentum (k-) space (which reduces to a sphere if $\varepsilon_1 = \varepsilon_2$, as shown in Fig. 2(a)). The absolute value of the k-vector in such a material is finite which leads to

* Corresponding author.
E-mail address: smoly@umd.edu (I.I. Smolyaninov).

http://dx.doi.org/10.1016/j.sse.2017.06.022
0038-1101/

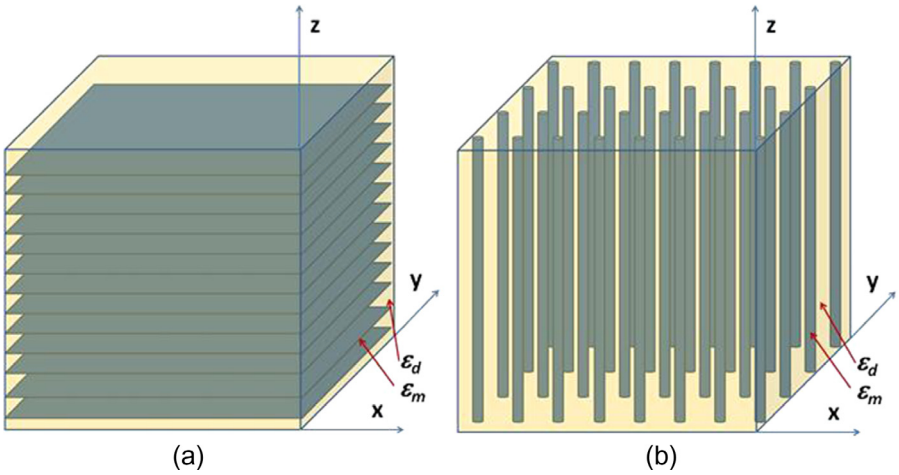

Fig. 1. Typical geometries of hyperbolic metamaterials: (a) multilayer metal-dielectric structure, and (b) metal wire array structure.

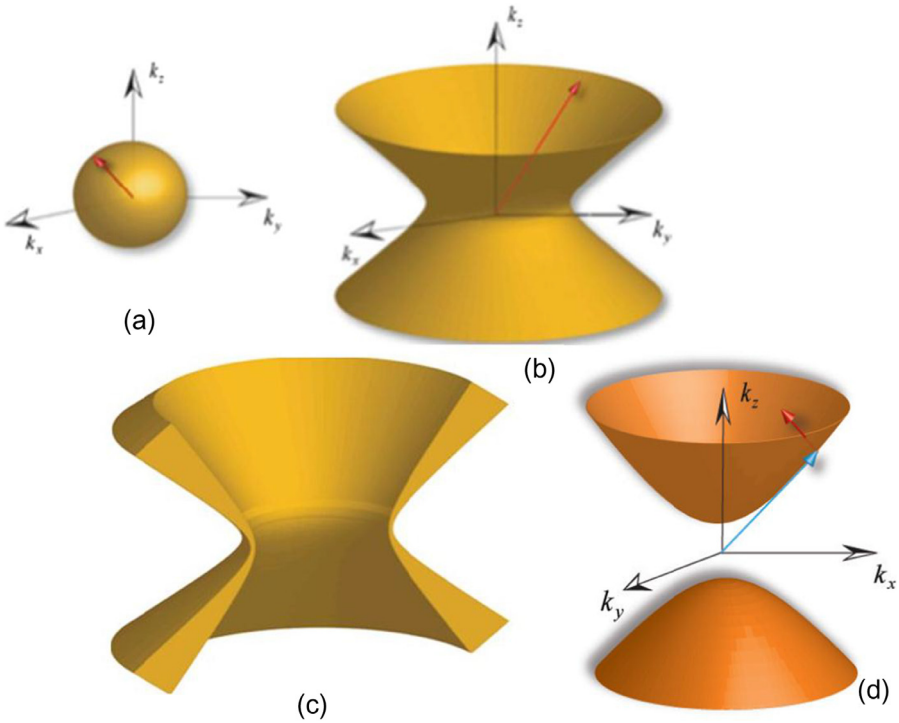

Fig. 2. The constant frequency surfaces for (a) isotropic dielectric ($\varepsilon_1 = \varepsilon_2 > 0$) and (b) uniaxial hyperbolic metamaterial in which $\varepsilon_x = \varepsilon_y = \varepsilon_1 > 0$ and $\varepsilon_z = \varepsilon_2 < 0$ (c) The phase space volume between two constant frequency surfaces for such a hyperbolic metamaterial. (d) The constant frequency surface for a uniaxial hyperbolic metamaterial in which $\varepsilon_x = \varepsilon_y = \varepsilon_1 < 0$ and $\varepsilon_z = \varepsilon_2 > 0$.

the usual diffraction limit on resolution of regular optics. The phase space volume enclosed between two such equi-frequency surfaces is also finite, corresponding to a finite density of photonic states. However, when one of the components of the dielectric permittivity tensor is negative, Eq. (2) describes a hyperboloid in the phase space (Fig. 2(b)). As a result, the absolute value of the k-vector is not limited, thus enabling super-resolution imaging with hyperbolic metamaterials. Moreover, the phase space volume between two such hyperboloids (corresponding to different values of frequency) is infinite (see Fig. 2(c)). The latter divergence leads to an infinite density of photonic states. While there are many mechanisms leading to a singularity in the density of photonic states, this one is unique as it leads to the infinite value of the density of states for every frequency where different components of the dielectric permittivity have opposite signs. It is this behavior which lies in the heart of the robust performance of hyperbolic metamaterials: while disorder can change the magnitude of the dielectric permittivity components, leading to a deformation of the corresponding hyperboloid in the phase (momentum) space, it will remain a hyperboloid and will therefore still support an infinite density of states. Such effective medium description will eventually fail at the point when the wavelength of the propagating mode becomes comparable to the size of the hyperbolic metamaterial unit cell a, introducing a natural wave number cut-off:

$$k_{\max} = 1/a \tag{3}$$

Depending on the metamaterial design and the fabrication method used, the unit cell size in optical metamaterials runs from $a \sim 10$ nm (in semiconductor [20] and metal-dielectric layered

structures [6]) to $a \sim 100$ nm (in nanowire composites [21,22]). Since the "hyperbolic" enhancement factor in the density of states [3] scales as

$$\rho(\omega) = \rho_0(\omega)\left(\frac{k_{\max}}{\omega/c}\right)^3 \tag{4}$$

where $\rho_0 \sim \omega^2$ is the free-space result, even with the cut-off taken into account, the hyperbolic singularity leads to the optical density of states enhancement by a factor of 10^3–10^5. Physically, the enhanced photonic density of states in the hyperbolic metamaterials originates from the waves with high wave numbers that are supported by the system. Such propagating modes that can achieve X-ray wavelengths at optical frequencies, do not have an equivalent in "regular" dielectrics where $k \leqslant \sqrt{\varepsilon}\omega/c$. Since each of these waves can be thermally excited, a hyperbolic metamaterial shows a dramatic enhancement in the radiative transfer rates.

As has been mentioned above, artificial hyperbolic metamaterials are typically composed of multilayer metal-dielectric or metal wire array structures, as shown in Fig. 1. For the multilayer geometry the diagonal components of the metamaterial permittivity can be calculated based on the Maxwell-Garnett approximation as follows:

$$\varepsilon_1 = \varepsilon_{xy} = n\varepsilon_m + (1-n)\varepsilon_d, \quad \varepsilon_2 = \varepsilon_z = \frac{\varepsilon_m\varepsilon_d}{(1-n)\varepsilon_m + n\varepsilon_d} \tag{5}$$

where n is the volume fraction of the metallic phase, and $\varepsilon_m < 0$ and $\varepsilon_d > 0$ are the dielectric permittivities of the metal and dielectric, respectively [23]. The validity of Maxwell-Garnett approximation has been clearly demonstrated in Ref. [23]. Analytical calculations based on the Maxwell-Garnett approximation performed for periodic array of metal nanolayers were confronted with exact numerical solutions of Maxwell equations. Excellent agreement between numerical simulations and analytical results was demonstrated. The Maxwell-Garnett approximation may also be used for a wire array metamaterial structure [23]. In this case the diagonal components of the permittivity tensor may be obtained as

$$\varepsilon_1 = \varepsilon_{x,y} = \frac{2n\varepsilon_m\varepsilon_d + (1-n)\varepsilon_d(\varepsilon_d+\varepsilon_m)}{(1-n)(\varepsilon_d+\varepsilon_m) + 2n\varepsilon_d}, \quad \varepsilon_2 = \varepsilon_z = n\varepsilon_m + (1-n)\varepsilon_d \tag{6}$$

Since both ε_m and ε_d depend on frequency, the frequency regions where ε_1 and ε_2 have opposite signs may be typically found for both multilayer and wire array geometries. Depending on the actual signs of ε_1 and ε_2, the phase space shape of the hyperbolic dispersion law may be either a one-sheet ($\varepsilon_2 > 0$ and $\varepsilon_1 < 0$, see Fig. 2(b)) or two-sheet ($\varepsilon_2 < 0$ and $\varepsilon_1 > 0$, see Fig. 2(d)) hyperboloid. However, in both cases the k-vector is not limited, and the photonic density of states exhibits broadband divergent behavior.

We should also note that it is relatively easy to emulate various 3D hyperbolic metamaterial geometries by planar plasmonic metamaterial arrangements. While rigorous description of such metamaterials in terms of Diakonov surface plasmons may be found in Ref. [24], qualitative analogy between 3D and 2D metamaterials may be explained as follows. A surface plasmon (SP) propagating over a flat metal-dielectric interface may be described by its well-known dispersion relation shown in Fig. 3.

$$k_p = \frac{\omega}{c}\left(\frac{\varepsilon_d\varepsilon_m}{\varepsilon_d+\varepsilon_m}\right)^{1/2} \tag{7}$$

where metal layer is considered to be thick, and $\varepsilon_m(\omega)$ and $\varepsilon_d(\omega)$ are the frequency-dependent dielectric constants of the metal and dielectric, respectively [25]. Thus, similar to the 3D case, we may introduce an effective 2D dielectric constant ε_{2D}, which characterizes the way in which SPs perceive the dielectric material deposited onto the metal surface. By requiring that $k_p = \varepsilon_{2D}{}^{1/2}\omega/c$, we obtain

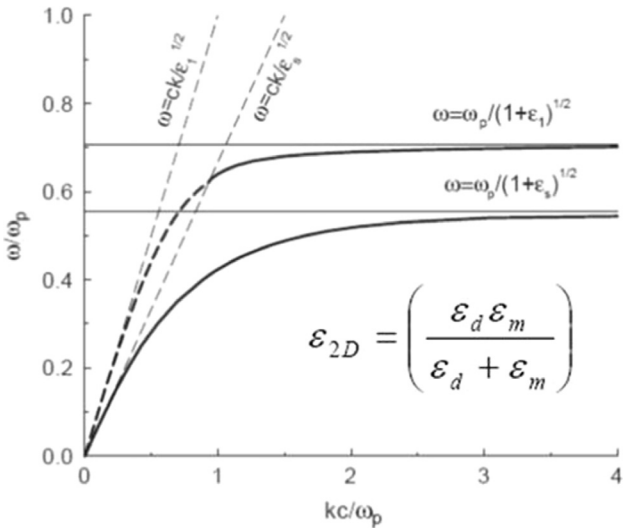

Fig. 3. Dispersion law of surface plasmon polaritons in the lossless approximation.

$$\varepsilon_{2D} = \left(\frac{\varepsilon_d\varepsilon_m}{\varepsilon_d+\varepsilon_m}\right) \tag{8}$$

Eq. (8) makes it obvious that depending on the plasmon frequency, SPs perceive the dielectric material bounding the metal surface (for example a PMMA layer) in drastically different ways. At low frequencies $\varepsilon_{2D} \approx \varepsilon_d$, so that plasmons perceive a PMMA layer as a dielectric. On the other hand, at high enough frequencies at which $\varepsilon_d(\omega) > -\varepsilon_m(\omega)$ (this happens around $\lambda_0 \sim 500$ nm for a PMMA layer) ε_{2D} changes sign and becomes negative. Thus, around $\lambda_0 \sim 500$ nm plasmons perceive a PMMA layer on gold as an "effective metal". As a result, around $\lambda_0 \sim 500$ nm plasmons perceive a PMMA stripe pattern on gold substrate as a layered hyperbolic metamaterial shown in Fig. 1(a). Fabrication of such plasmonic hyperbolic metamaterials in two dimensions requires only very simple and common lithographic techniques [4].

2. Super-resolution imaging using hyperbolic metamaterials: the hyperlens

Although various electron and scanning probe microscopes have long surpassed the conventional optical microscope in resolving power, optical microscopy remains invaluable in many fields of science. The practical limit to the resolution of a conventional optical microscope is determined by diffraction: a wave cannot be localized to a region much smaller than half of its vacuum wavelength $\lambda_0/2$. Immersion microscopes introduced by Abbé in the 19th century have slightly improved resolution, on the order of $\lambda_0/2n$ because of the shorter wavelength of light λ_0/n in a medium with refractive index n. However, immersion microscopes are limited by the small range of refractive indices n of available transparent materials. For a while it was believed that the only way to achieve nanometer-scale spatial resolution in an optical microscope was to detect evanescent optical waves in very close proximity to a studied sample using a near-field scanning optical microscope (NSOM) [26]. However, progress in metamaterials demonstrated quite a few ways to achieve similar resolution using traditional non-scanning imaging.

An important early step to overcome this limitation was made in surface plasmon-assisted microscopy experiments [27], in which two-dimensional (2D) image magnification was achieved. In this microscope design the dispersion behavior of SPPs propagating in the boundary between a thin metal film and a dielectric

(7) was exploited to use the 2-D optics of SPPs with a short wavelength to produce a magnified local image of an object on the surface. The increased spatial resolution of microscopy experiments performed with SPPs [27] is based on the "hyperbolic" dispersion law of such waves, which may be written in the form

$$k_{xy}^2 - |k_z|^2 = \frac{\varepsilon_d \omega^2}{c^2} \tag{9}$$

where ε_d is the dielectric constant of the medium bounding the metal surface, which for air is = 1, $k_{xy} = k_p$ is the wave vector component in the plane of propagation, and k_z is the wave vector component perpendicular to the plane. This form of the dispersion relation originates from the exponential decay of the surface wave field away from the propagation plane.

The "optical hyperlens" design described by Jacob et al. [2] extends this idea by using a hyperbolic metamaterial made of a concentric arrangement of metal and dielectric cylinders, which may be characterized by a strongly anisotropic dielectric permittivity tensor in which the tangential ε_θ and the radial ε_r components have opposite signs. The resulting hyperbolic dispersion relation

$$\frac{k_r^2}{\varepsilon_\theta} - \frac{k_\theta^2}{|\varepsilon_r|} = \frac{\omega^2}{c^2} \tag{10}$$

does not exhibit any lower limit on the wavelength of propagating light at a given frequency. Therefore, in a manner similar to the 2D optics of SPPs, there is no usual diffraction limit in this metamaterial medium. Abbe's resolution limit simply does not exist. Optical energy propagates through such a metamaterial in the form of radial rays. Moreover, as demonstrated in Section 1, a pattern of polymethyl methacrylate (PMMA) stripes formed on a metal surface (as shown in Fig. 4) behaves as a 2D plasmonic equivalent of 3D hyperbolic metamaterial. Thus, a plasmon microscope may be operated in the "hyperlens mode" (Fig. 4) in which the plasmons generated by the sample located in the center of the plasmonic hyperlens propagate in the radial direction. The lateral distance between plasmonic rays grows with distance along the radius. The images are viewed by a regular microscope.

The internal structure of the magnifying hyperlens (Fig. 5(a)) consists of concentric rings of PMMA deposited on a gold film surface. The required concentric structures were defined using a Raith E-line electron beam lithography (EBL) system with ~70 nm spatial resolution. The written structures were subsequently developed using a 3:1 IPA/MIBK solution (Microchem) as developer and imaged using AFM (see Fig. 4). According to theoretical proposals in Refs. [1,2], optical energy propagates through a hyperbolic metamaterial in the form of radial rays. This behavior is clearly demonstrated in Fig. 5(b). If point sources are located near the inner rim of the concentric metamaterial structure, the lateral separation of the rays radiated from these sources increases upon propagation towards the outer rim. Therefore, resolution of an "immersion" microscope (a hyperlens) based on such a metamaterial structure is defined by the ratio of inner to outer radii. Resolution appears limited only by losses, which can be compensated by optical gain. The magnifying superlenses (or hyperlenses) have been independently realized for the first time in two experiments [4,5]. In particular, experimental data obtained using a 2D plasmonic hyperlens (shown in Fig. 5(a)) do indeed demonstrate ray-like propagation of subwavelength plasmonic beams emanated by test samples.

We should also note that similar to 3D optics, hyperbolic and negative index behaviours typically coexist in plasmonic metamaterials (see [4] and the inset in Fig. 4), the latter often leading to self-imaging effects. A new example of such self-imaging effect in a PMMA-based plasmonic metamaterial is presented in Fig. 6. It demonstrates self-imaging due to negative refraction in a 2D plasmonic crystal illuminated with $\lambda = 532$ nm laser light. Rows of triangles (2 μm on the side) have been produced in a 150 nm thick PMMA film deposited on top of a 50 nm thick gold film surface using E-beam lithography. Relatively large periodicity D of triangles in this pattern compared to the illumination wavelength lets us clearly distinguish this NIM-induced self-imaging behavior from the Talbot effect, which would produce images at $D^2/\lambda \sim 50$ μm distance from the edge of the triangular pattern.

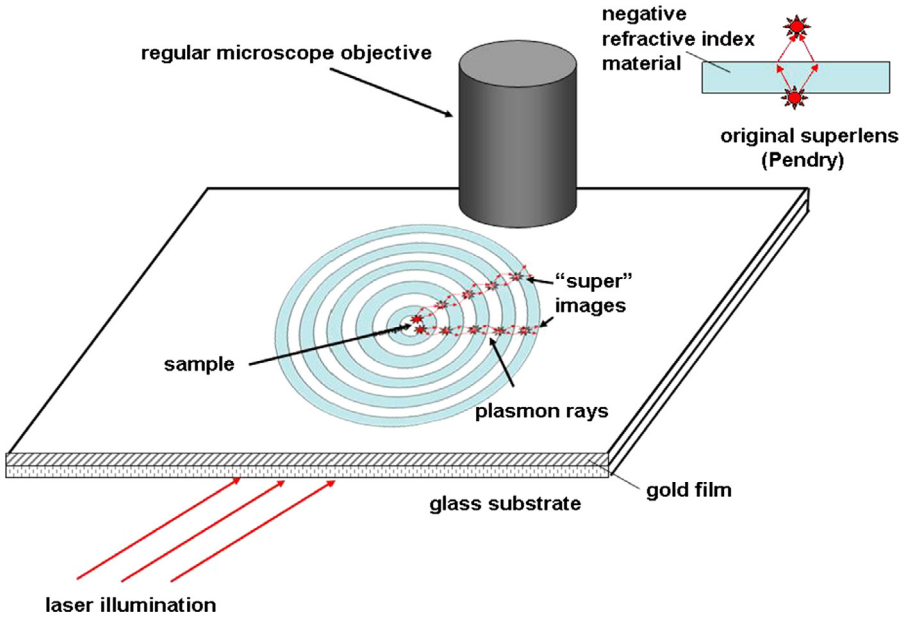

Fig. 4. Plasmon microscope operating in the "hyperlens mode": the plasmons generated by the sample located in the center of the hyperlens propagate in the radial direction. The lateral distance between plasmonic rays grows with distance along the radius. The images are viewed by a regular microscope.

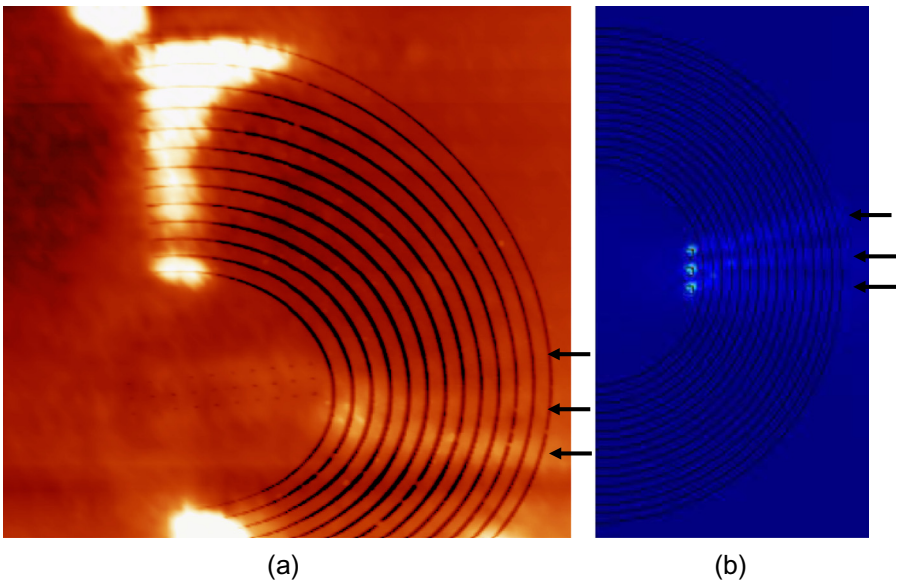

Fig. 5. (a) Superposition image composed of an AFM image of the PMMA on gold plasmonic metamaterial structure superimposed onto the corresponding optical image obtained using a conventional optical microscope illustrating the imaging mechanism of the magnifying hyperlens. Near the edge of the hyperlens the separation of three rays (marked by arrows) is large enough to be resolved using a conventional optical microscope. (b) Theoretical simulation of ray propagation in the magnifying hyperlens microscope.

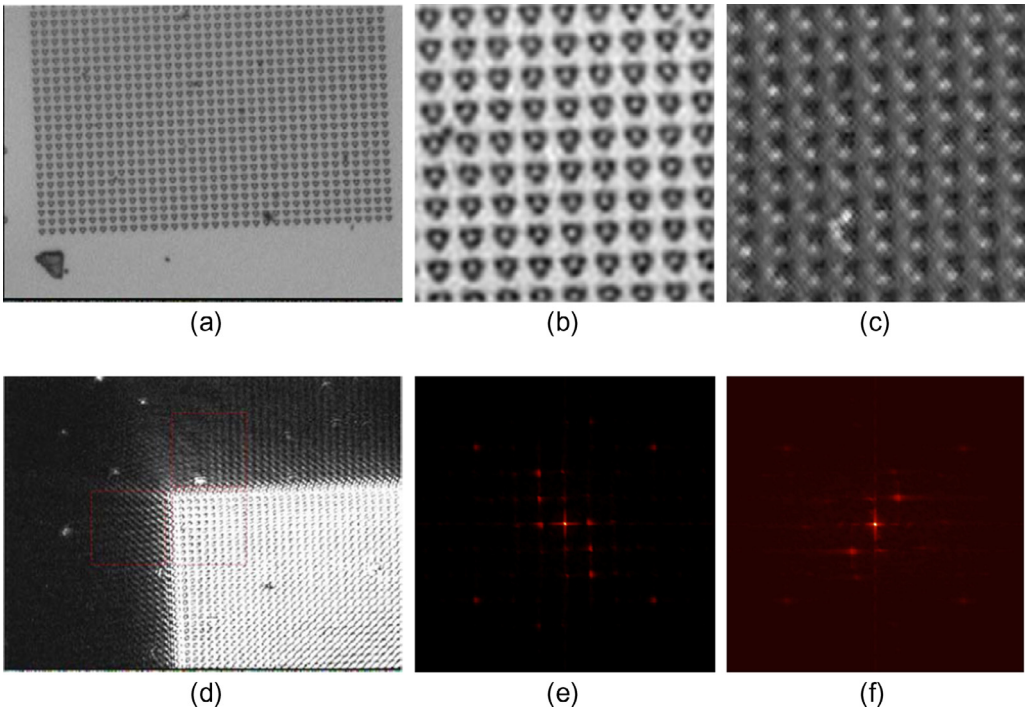

Fig. 6. Self-imaging of triangular pattern due to negative index behavior of the PMMA-based plasmonic crystal: (a and b) Geometry of the plasmonic crystal at different magnifications. (c) Illumination at oblique angle produces non-mirror symmetric field distribution inside the plasmonic crystal (d) Self-imaging of the structure due to negative index behavior is evident from the mirror symmetry of the FFT maps of the object (e) and the image (f).

3. Consequences of singular photonic density of states: radiative decay engineering, thermal hyper-conductivity, and new stealth technologies

As we discussed in Section 1, the broadband divergence of photonic density of states in hyperbolic metamaterial is unique since it leads to the infinite value of the density of states for every frequency where different components of the dielectric permittivity have opposite signs. This very large number of electromagnetic states can couple to quantum emitters leading to such unusual phenomena as the broadband Purcell effect [6] and thermal hyperconductivity [10]. On the other hand, free space photons illuminating a roughened surface of hyperbolic metamaterial preferentially scatter inside the metamaterial leading to the surface being "darker than black" at the hyperbolic frequencies [9]. The latter property may find natural applications in stealth technologies.

As a first example of these unusual quantum behaviours, let us consider the broadband Purcell effect, which may become extremely useful for such applications as single photon sources, fluorescence imaging, biosensing and single molecule detection. In the spirit of the Fermi's golden rule, an increased number of radiative decay channels due to the high-k states in hyperbolic media (available for an excited atom) must ensure enhanced spontaneous emission. This enhancement can increase the quantum yield by overcoming emission into competing non-radiative decay routes such as phonons. A decrease in lifetime, high quantum yield and good collection efficiency can lead to extraction of single photons reliably at a high repetition rate from isolated emitters [28]. The available radiative channels for the spontaneous photon emission consist of the propagating waves in vacuum, the plasmon on the metamaterial substrate and the continuum of high wave vector waves which are evanescent in vacuum but propagating within the metamaterial. The corresponding decay rate into the metamaterial modes when the emitter is located at a distance $a < d \ll \lambda$ (where a is the metamaterial patterning scale) is [6]

$$\Gamma^{meta} \approx \frac{\mu^2}{2\hbar d^3} \frac{2\sqrt{\varepsilon_x|\varepsilon_z|}}{(1+\varepsilon_x|\varepsilon_z|)} \tag{11}$$

In the close vicinity of the hyperbolic metamaterial, the power from the dipole is completely concentrated in the large spatial wave vector channels (Fig. 7(a) inset). The same evanescent wave spectrum when incident on a lossy metal or dielectric would be completely absorbed, causing a non-radiative decrease in the lifetime of an emitter (quenching). On the contrary, the metamaterial converts the evanescent waves to propagating and the absorption thus affects the out-coupling efficiency of the emitted photons due to a finite propagation length in the metamaterial.

Along with the reduction in lifetime and high efficiency of emission into the metamaterial, another key feature of the hyperbolic media is the directional nature of light propagation [6]. Fig. 7(b) shows the field along a plane perpendicular to the metamaterial-vacuum interface exhibiting the beamlike radiation from a point dipole. This is advantageous from the point of view of collection efficiency of light since the spontaneous emitted photons lie within a cone. The group velocity vectors in the medium which point in the direction of the Poynting vector are simply normals to the dispersion curve. For vacuum, these normals point in all directions and hence the spontaneous emission is isotropic in nature. In contrast to this behavior, the hyperbolic dispersion medium allows wave vectors only within a narrow region defined by the asymptotes of the hyperbola. Hence the group velocity vectors lie within the resonance cone giving rise to a directional spontaneously emitted photon propagating within the metamaterial. This effect has been demonstrated in experiments with PMMA-based plasmonic hyperbolic metamaterial samples (similar to the one shown in Fig. 5(a)). The PMMA used in metamaterial fabrication was doped with fluorescein dye. As demonstrated in Fig. 7(c), fluorescence in such metamaterial samples indeed appears to be strongly directional.

Since its theoretical prediction in [6], the broadband Purcell effect has been indeed observed in multiple experiments, such as

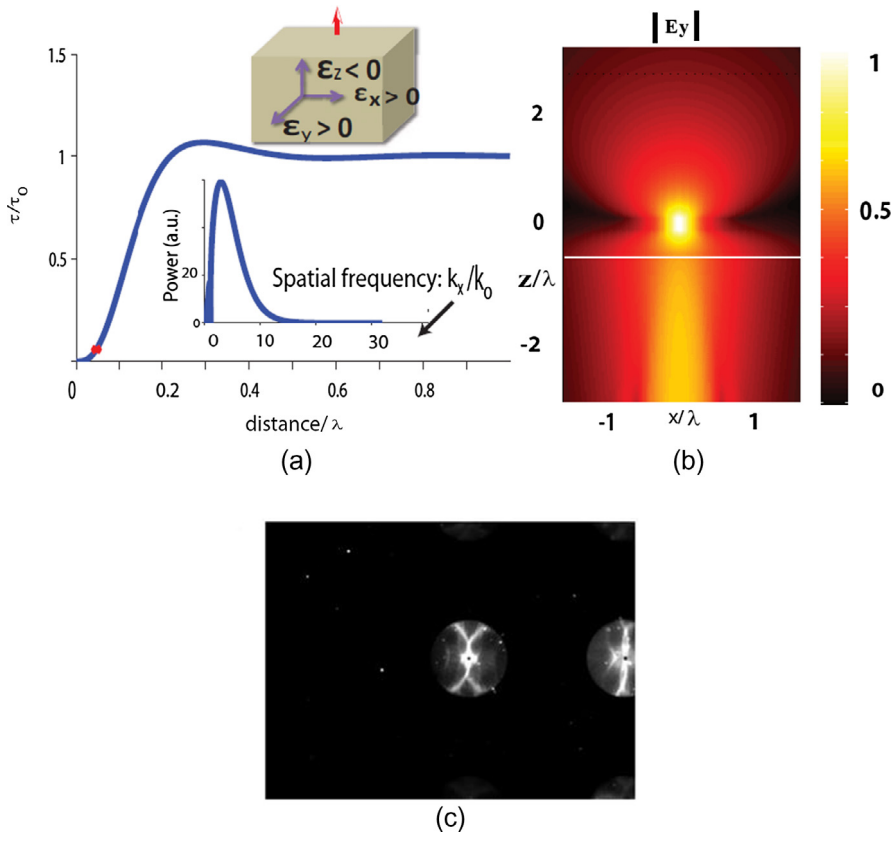

Fig. 7. (a) Spontaneous emission lifetime of a perpendicular dipole above a hyperbolic metamaterial substrate (see inset). Note the lifetime goes to zero in the close vicinity of the metamaterial as the photons are emitted nearly instantly. Most of the power emitted by the dipole is concentrated in the large spatial modes (evanescent in vacuum) which are converted to propagating waves within the metamaterial. (inset) (b) False color plot of the field of the point dipole in a plane perpendicular to the metamaterial-vacuum interface (see inset of (a)) depicting the highly directional nature of the spontaneous emission (resonance cone). (c) Experimental demonstration of directional fluorescence in the PMMA-based plasmonic hyperbolic metamaterial sample (similar to the one shown in Fig. 5(a)). The PMMA used in metamaterial fabrication was doped with fluorescein dye.

[7,8]. Virtually the same physics as in Fig. 6(b) is also responsible for the "darker than black" behavior of roughened hyperbolic metamaterials [9]. Free space photons illuminating a rough surface of the hyperbolic metamaterial preferentially scatter inside the metamaterial into the bulk high k-vector modes. As a result, the photon probability to scatter back into free space is almost zero and the roughened surface looks black in the hyperbolic frequency bands.

Let us now consider radiative heat transfer inside hyperbolic metamaterials. It appears that the broadband divergence of the photonic density of states described above also leads to giant increase in radiative heat transfer compared to the Stefan-Boltzmann law in vacuum and in usual anisotropic dielectric materials. According to numerical calculations [10], this radiative thermal "hyperconductivity" may approach or even exceed heat conductivity via electrons and phonons in regular solids with the additional advantage of radiative heat transfer being much faster. Therefore, this radiative thermal hyperconductivity may potentially be very useful in fast microelectronics heat management applications [29]. In such applications heat generated by micro and nanoelectronic circuit components needs to be quickly dissipated at a heat sink, which cannot be located in the immediate vicinity of the electronic component. A hyperbolic metamaterial heat management layer may solve this important technological problem.

Let us start by tracing how the photonic density of states enters the usual Stefan-Boltzmann law. For the sake of simplicity, we will consider vacuum as a typical example of "normal" or "elliptical" material. As usual, we can start by calculating energy density of the black body radiation. A well-known textbook derivation can be summarized as follows:

$$u_{ell} = \frac{U}{V} = \int_0^\infty \frac{\varepsilon}{\exp\left(\frac{\varepsilon}{kT}\right) - 1} g(\varepsilon) d\varepsilon = \frac{4\sigma T^4}{c} \tag{12}$$

where $g(\varepsilon)$ is the photonic density of states. Eq. (12) clearly demonstrates that the drastic change in the density of states schematically shown in Fig. 8 must lead to the drastic change in the final result. The singular behavior of the photonic density of states in hyperbolic metamaterial takes these media beyond the realm of the Stefan-Boltzmann law, with no ultimate limit on the radiative heat transfer. For the energy flux along the symmetry axis of a uniaxial hyperbolic metamaterial, it was found [10] that

$$S_T = \frac{\hbar c^2 k_{\max}^4}{32\pi^2} \int d\omega \frac{1}{\exp\left(\frac{\hbar\omega}{kT}\right) - 1} \left| \frac{\varepsilon_1 \frac{d\varepsilon_2}{d\omega} - \varepsilon_2 \frac{d\varepsilon_1}{d\omega}}{\det \|\varepsilon\|} \right| \tag{13}$$

where the frequency integration is taken over the frequency bandwidth corresponding to the hyperbolic dispersion. Note that the heat flux in Eq. (13) is very sensitive to the dispersion in the hyperbolic metamaterial, $d\varepsilon/d\omega$. Indeed, the derivative of the dielectric permittivity determines the difference in the asymptotic behavior of the k-vector between the two hyperbolic surfaces that determine the phase space volume between the frequencies ω and $\omega + d\omega$ (see Fig. 8), and thus defines the actual value of the density of states. While there are many metamaterial designs leading to the hyperbolic dispersion, the most practical and widely used systems rely on either the medal-dielectric layer approach, or incorporate aligned metal nanowire composites (as shown in Fig. 1). For the planar layers design, the hyperbolic behavior is observed for the wavelengths above ~10 μm, if the system is fabricated using semiconductors [20], or for the wavelength above ~1 μm if the metamaterial is composed of metal-dielectric layers [7]. For the nanowire based approach, the hyperbolic dispersion is present at $\lambda > 1$ μm [21]. As a result, with either of these conventional metamaterial designs, the desired hyperbolic behavior covers the full range of wavelength relevant for the radiative heat transfer. As a result,

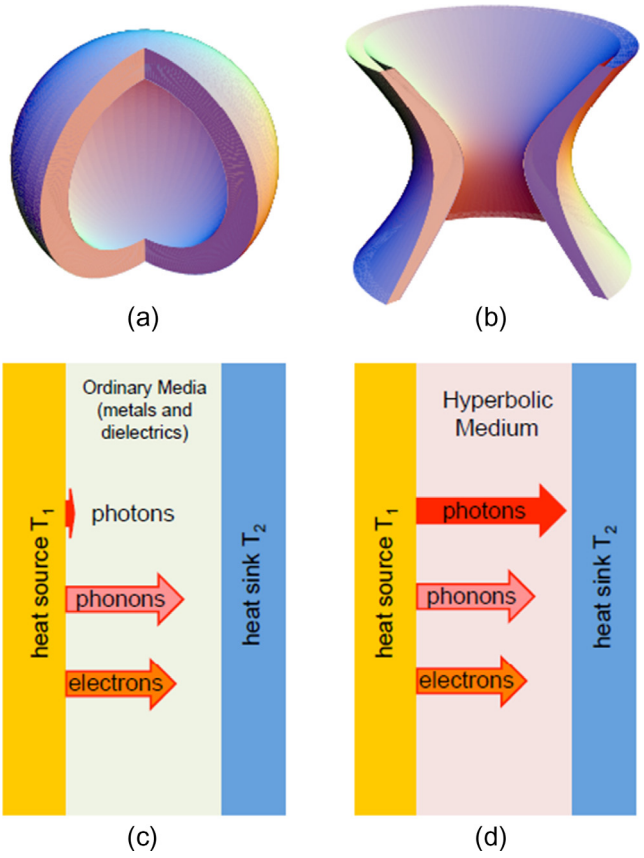

Fig. 8. The phase space volume between two constant frequency surfaces for (a) dielectric (elliptical) and (b) hyperbolic material with $\varepsilon_2 > 0$ and $\varepsilon_1 < 0$ (cut-out view). Panels (c) and (d) schematically illustrate different thermal conductivity mechanisms in (c) regular media (metals and dielectric) and (d) hyperbolic media. Giant radiative contribution to thermal conductivity in hyperbolic media can dominate the thermal transport.

the following estimates on the thermal energy flux in hyperbolic metamaterials have been obtained [10]:

$$S_T \approx \frac{\varepsilon_d}{4(1-n)} S_T^{(0)} \left(\frac{k_{\max}}{k_p}\right)^4 \tag{14}$$

for the layered material design, and

$$S_T \approx \frac{5}{16\pi^2} S_T^{(0)} \left(\frac{k_{\max}^2}{k_T k_p}\right)^2 \tag{15}$$

for the wire array design, where $S^{(0)}{}_T$ is the blackbody thermal energy flux for emission into the free space, k_p is the plasma momentum, k_T is the thermal momentum, and k_{max} is the structural parameter of the metamaterial defined by its periodicity. In both cases the numerical values of S_T exceed $S^{(0)}{}_T$ by 4 to 5 orders of magnitude, thus firmly placing hyperbolic metamaterials in the realm of practical applications for radiative heat transfer and thermal management. A similar enhancement may be also expected in thermal conductivity.

Using the ideas described above, we have developed a novel VCSEL geometry (see Fig. 9), in which the Bragg mirrors may be engineered in such a way that they exhibit hyperbolic metamaterial properties in the long wavelength infrared (LWIR) range [29]. As a result, such hyperbolic Bragg mirrors may be used to efficiently remove excess heat from the laser cavity, while in the near IR range both materials in the pair used for the Bragg mirror remain very good low loss dielectrics. Examples of such materials

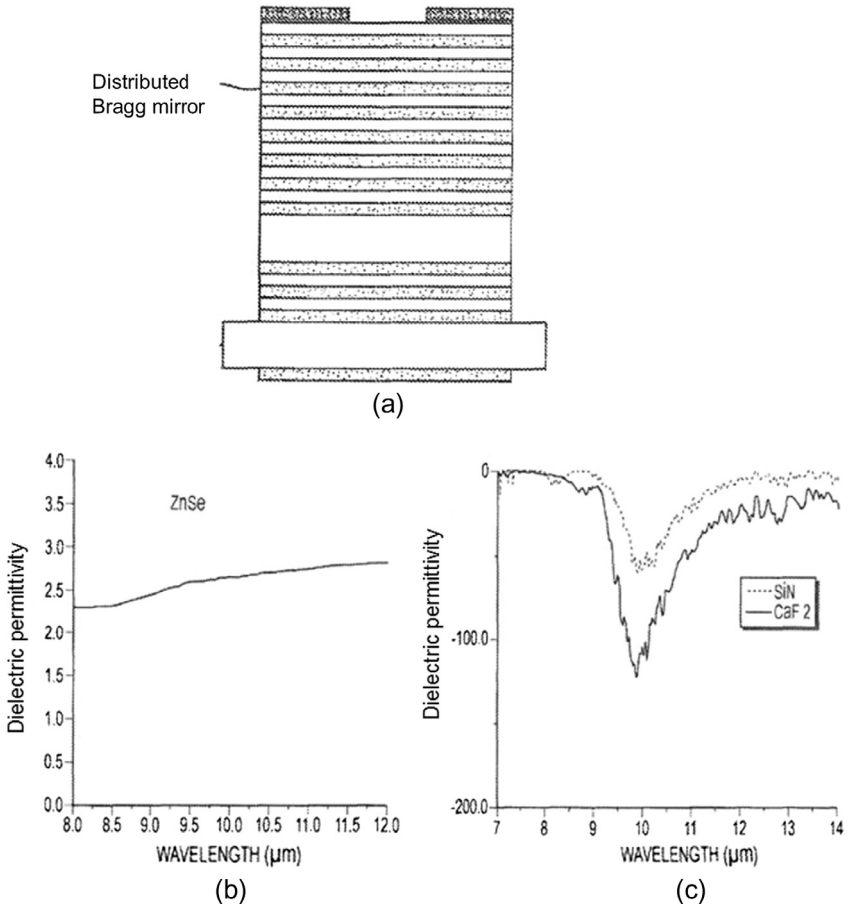

Fig. 9. (a) Bragg mirror, which acts as a hyperbolic metamaterial removes heat from the active region of a VCSEL [29]. (b) ZnSe has positive dielectric constant across the LWIR spectral range. (c) Both SiN and CaF_2 exhibit negative dielectric constant in a portion of LWIR range.

are shown in Fig. 9(b) and (c). For example, ZnSe has positive dielectric constant across the LWIR spectral range, while either SiN or CaF_2 may be used as a "negative material" in the pair, since both materials exhibit negative dielectric constant in a large portion of the LWIR range. The thermal energy flux enhancement for this design of the Bragg mirror may be estimated using Eq. (15). Since in this layered hyperbolic geometry $k_p \sim k_T$, and the structural parameter of the metamaterial k_{max} is an order of magnitude larger, four orders of magnitude enhancement may be expected in the thermal energy flux.

4. Self-assembled photonic hypercrystals

Explosive development of research on hyperbolic metamaterial also resulted in the recent demonstration of a novel artificial optical material, the "photonic hyper-crystal" [30], which combines the most interesting features of hyperbolic metamaterials and photonic crystals. Similar to hyperbolic metamaterials, photonic hyper-crystals exhibit broadband divergence in their photonic density of states due to the lack of usual diffraction limit on the photon wave vector. On the other hand, similar to photonic crystals, hyperbolic dispersion law of extraordinary photons is modulated by forbidden gaps near the boundaries of photonic Brillouin zones. Three dimensional self-assembly of photonic hyper-crystals has been achieved by application of external magnetic field to a cobalt nanoparticle-based ferrofluid. Unique spectral properties of photonic hyper-crystals lead to extreme sensitivity of the material to monolayer coatings of cobalt nanoparticles, which should find numerous applications in biological and chemical sensing.

Over the last few decades a considerable progress has been made in developing artificial optical materials with novel and often counterintuitive properties. Revolutionary research by Yablonovitch and John on photonic crystals [31,32] was followed by the development of electromagnetic metamaterial paradigm by Pendry [33]. Even though considerable difficulties still exist in fabrication of three-dimensional (3D) photonic crystals and metamaterials, both fields exhibit considerable experimental progress [34,35]. On the other hand, on the theoretical side these fields are believed to be complementary but mutually exclusive. Photonic crystal effects typically occur in artificial optical media which are periodically structured on the scale of free space light wavelength λ, while electromagnetic metamaterials are required to be structured (not necessarily in a periodic fashion) on the scale, which is much smaller than the free space wavelength of light. For example, in metal nanowire-based hyperbolic metamaterials schematically shown in Fig. 1(b) the inter-wire distance must be much smaller than λ. Experimental realization of 3D "photonic hyper-crystals" [30] bridges this divide by combining the most interesting properties of hyperbolic metamaterials and photonic crystals.

The concept of the photonic hyper-crystal is based on the fact that dispersion law of extraordinary photons in hyperbolic metamaterials (2) does not exhibit the usual diffraction limit. Existence of large k-vector modes in a broad range of frequencies means that periodic modulation of hyperbolic metamaterial properties on a scale $L \ll \lambda$ (see inset in Fig. 10(a)) would lead to Bragg scattering

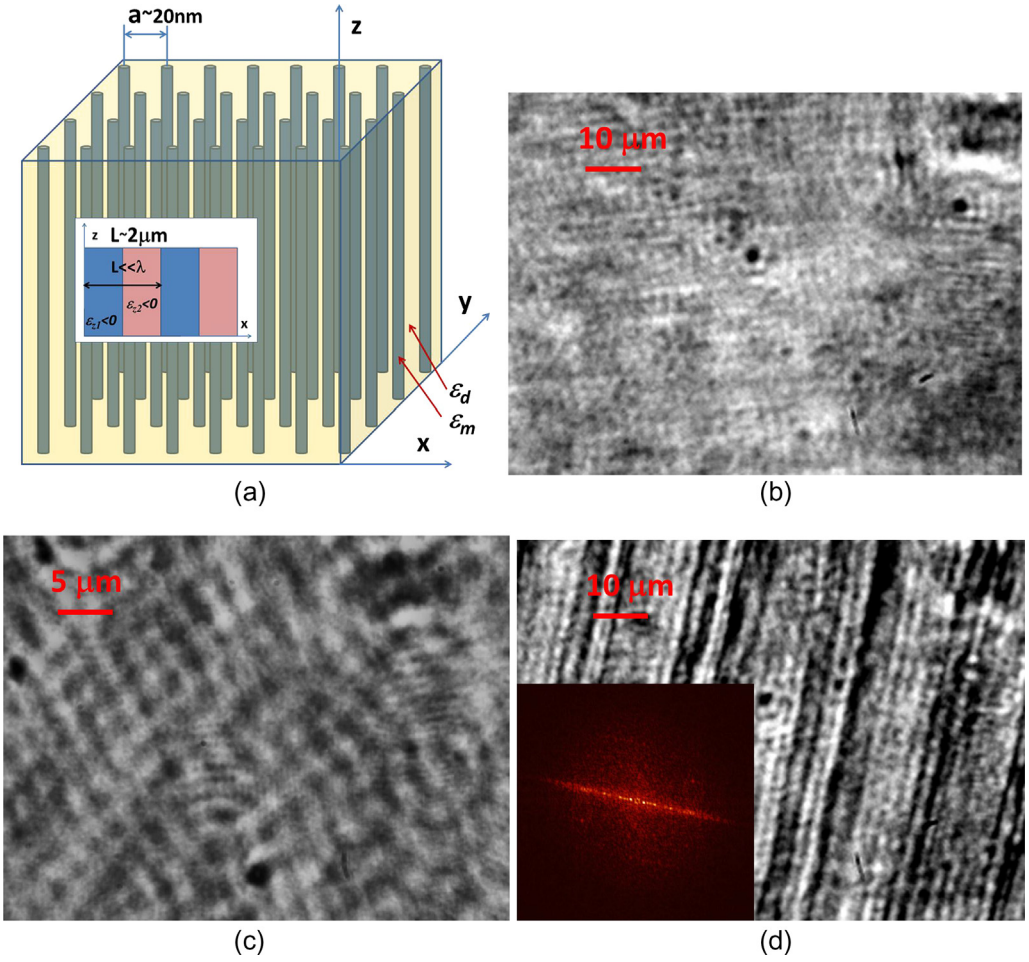

Fig. 10. (a) Experimental geometry of the ferrofluid-based hyperbolic metamaterial. The array of self-assembled cobalt nanocolumns has typical separation $a \sim 20$ nm between the nanocolumns. The inset shows a photonic hyper-crystal structure formed by periodic arrangement of cobalt rich and cobalt sparse regions with typical periodicity $L \sim 2$ μm, so that periodic modulation of hyperbolic metamaterial properties on a scale $L \ll \lambda$ is achieved in the LWIR spectral range where $\lambda \sim 10$ μm. Since photon wave vector in hyperbolic metamaterials is not diffraction-limited, periodic modulation of hyperbolic metamaterial properties on a scale $L \ll \lambda$ would lead to Bragg scattering and formation of band structure. (b–d) Microscopic images of cobalt nanoparticle-based ferrofluid reveal subwavelength modulation of its spatial properties: frames (b) and (d) show microscopic images of the diluted cobalt nanoparticle-based ferrofluid before and after application of external magnetic field. The pattern of self-assembled stripes visible in image (d) is due to phase separation of the ferrofluid into cobalt reach and cobalt poor phases. The stripes are oriented along the direction of magnetic field. The inset shows Fourier transform image of frame (d).

of extraordinary photons and formation of photonic band structure no matter how small L is [30]. Thus, so formed "photonic hyper-crystals" would combine the most interesting properties of hyperbolic metamaterials and photonic crystals. For example, similar to classic photonic crystal effect predicted by John [32], strong localization of photons may occur in photonic hyper-crystals. However, unlike usual photonic crystals where light localization occurs on a scale $\sim\lambda$, photonic hyper-crystals may exhibit light localization on deep subwavelength scale. Similar to surface plasmon resonance (SPR) [25] and surface enhanced Raman (SERS) [36] - based sensing, engineered localization of light on deep subwavelength scale in photonic hyper-crystals should find numerous applications in biological and chemical sensing.

Validation of the photonic hyper-crystal concept has been achieved using an experimental technique based on three-dimensional self-assembly of cobalt nanoparticles in the presence of external magnetic field [30]. Magnetic nanoparticles in a ferrofluid are known to form nanocolumns aligned along the magnetic field [37]. Moreover, depending on the magnitude of magnetic field, nanoparticle concentration and solvent used, phase separation into nanoparticle rich and nanoparticle poor phases may occur in many ferrofluids [38]. This phase separation occurs on a 0.1–1 μm scale. Therefore, it can be used to fabricate a self-assembled photonic hypercrystal.

These experiments used cobalt magnetic fluid 27–0001 from Strem Chemicals composed of 10 nm cobalt nanoparticles in kerosene coated with sodium dioctylsulfosuccinate and a monolayer of LP4 fatty acid condensation polymer. The average volume fraction of cobalt nanoparticles in this ferrofluid is p = 8.2%. Cobalt behaves as an excellent metal in the long wavelength infrared range (LWIR: the real part of its refractive index, n, is much smaller than its imaginary part, k [39]. Thus, real part of ε, $\mathrm{Re}\varepsilon = n^2 - k^2$, is negative, and its absolute value is much larger than its imaginary part, $\mathrm{Im}\varepsilon = 2nk$. Therefore, it is highly suitable for fabrication of hyperbolic metamaterials. The structural parameter of such a metamaterial falls into a few nanometers range: the cobalt nanoparticle size is 10 nm, while average inter-particle distance at 8.2% volume fraction is about 19 nm. Therefore, the metamaterial properties may be described by effective medium parameters on spatial scales ~100 nm. On the other hand, ferrofluid begins to exhibit hyperbolic behavior in the range of free space wavelengths ~10 μm and above - in the so called long wavelength infrared (LWIR) frequency range. Thus, in between 100 nm and 10,000 nm there exists an ample range of spatial scales which enable photonic

hyper-crystal behavior described above. For example, if the effective medium parameters of ferrofluid are modulated on the scale of ~2000 nm (as evident from Fig. 10(d)) the large k-vector modes which exist in the metamaterial in the LWIR range will experience Bragg scattering due to this modulation. Indeed, a diluted ferrofluid develops very pronounced phase separation into periodically aligned cobalt rich and cobalt poor phases (with periodicity L ~2 μm) if subjected to external magnetic field. Optical microscope images of the diluted ferrofluid before and after application of external magnetic field are shown in Fig. 10(b) and (d). The periodic pattern of self-assembled stripes visible in image (d) appears due to phase separation. The stripes are oriented along the direction of magnetic field. The stripe periodicity $L \sim 2$ μm appears to be much smaller than the free space wavelength in the hyperbolic frequency range. Therefore, created self-assembled optical medium appears to be a photonic hyper-crystal.

Polarization dependencies of ferrofluid transmission as a function of magnetic field and nanoparticle concentration measured in a broad 0.5–16 μm wavelength range conclusively prove hyperbolic crystal character of ferrofluid anisotropy in the long wavelength IR range at large enough magnetic field. Fig. 11 shows polarization-dependent transmission spectra of 200 μm thick undiluted ferrofluid sample obtained using FTIR spectrometer. These data are consistent with hyperbolic character of ε tensor of the ferrofluid in $B = 1000$ G. Ferrofluid transmission is large for polarization direction perpendicular to magnetic field (perpendicular to cobalt nanoparticle chains) suggesting dielectric character of ε in this direction. On the other hand, ferrofluid transmission falls to near zero for polarization direction along the chains, suggesting metallic character of ε in this direction. However, these measurements are affected by numerous ferrofluid absorption lines.

Fabricated photonic hyper-crystals exhibit all the typical features associated with the hyperbolic metamaterials. For example, absorption spectra measured using FTIR spectrometer with and without external magnetic field are consistent with the decrease of the radiation lifetime of kerosene molecules in the hyperbolic state [30]. Moreover, FTIR spectral measurements are broadly accepted as a powerful "chemical fingerprinting" tool in chemical and biosensing [40]. Therefore, broadly available magnetic field-tunable photonic hyper-crystals operating in the IR range open up new valuable opportunities in chemical analysis. Fig. 12 clearly illustrates the photonic hyper-crystal potential in chemical and biological sensing by detailed measurements of magnetic field induced FTIR transmission of the ferrofluid. Fig. 12 shows FTIR transmission measurements in the 2100–2500 cm^{-1} spectral range of the kerosene-based ferrofluid in which 10% of toluene has been added by volume with and without the external magnetic field. As indicated by an arrow, self-assembly of the ferrofluid into a hyperbolic metamaterial leads to sharp modification of the ferrofluid absorption spectrum in the range of characteristic toluene absorption lines. As demonstrated in [30], this magnetic field induced effect may be attributed to field enhancement by cobalt nanoparticle chains. We expect that further optimization of photonic hyper-crystals geometry will lead to much stronger sensitivity of their optical properties to chemical and biological inclusions, indicating a very strong potential of photonic hyper-crystals in biological and chemical sensing.

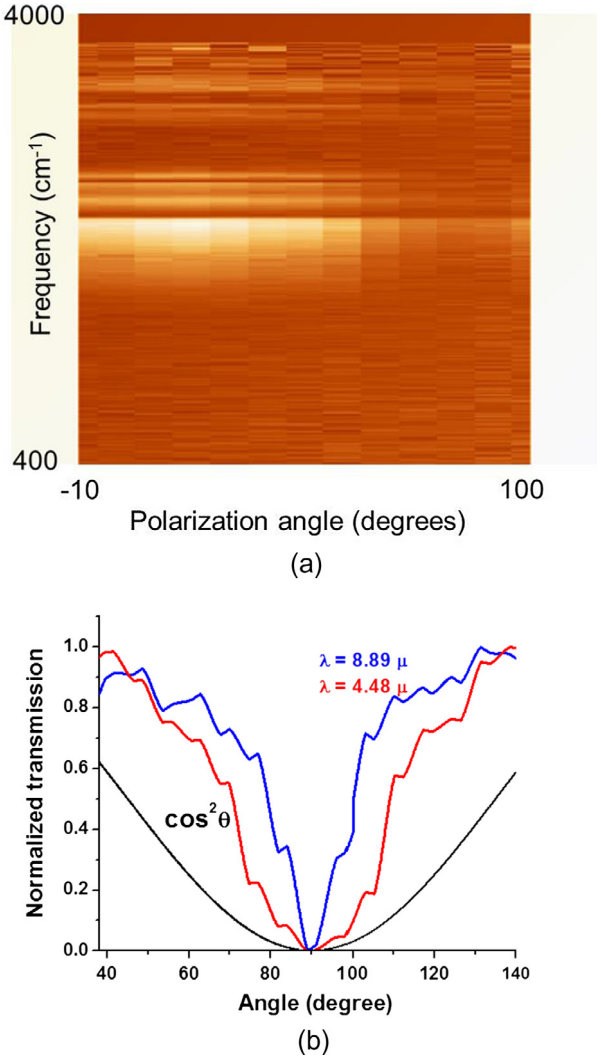

Fig. 11. Polarization-dependent transmission spectra of 200 μm - thick ferrofluid sample measured using FTIR spectrometer are consistent with hyperbolic character of ε tensor: (a) Two-dimensional representation of ferrofluid transmission (shown via pixel brightness) measured using polarization-sensitive FTIR spectrometer as a function of IR wavelength and polarization. (b) Transmission data as a function of polarization angle for $\lambda = 8.89$ μm and 4.48 μm exhibiting deviation from Malus law, $\cos^2\phi$ (black line), which is typical for photonic hypercrystals [30].

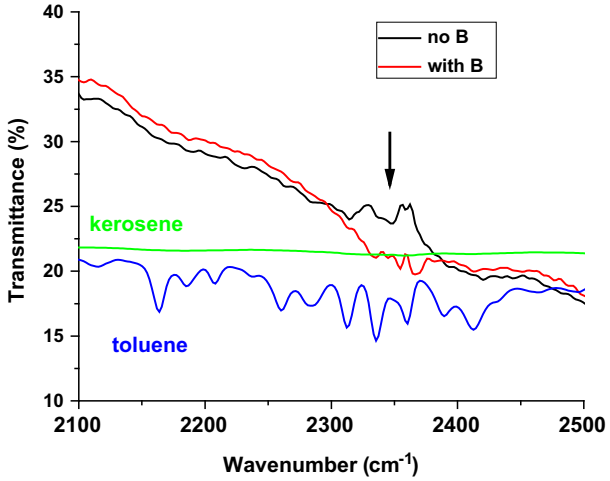

Fig. 12. FTIR transmission spectra of kerosene, toluene, and the kerosene-based ferrofluid with addition of 10% toluene measured with and without the external magnetic field in the 2100–2500 cm^{-1} spectral range. As indicated by an arrow, self-assembly of the ferrofluid into a hyperbolic metamaterial leads to sharp modification of the ferrofluid absorption spectrum in the range of toluene absorption lines.

5. Conclusions

The diverse physical properties and applications of hyperbolic metamaterials outlined above clearly demonstrate that this subfield of electromagnetic metamaterials already extended far beyond its original goal to enable sub-diffraction superresolution imaging. While imaging applications progress at a very high speed [41–43], hyperbolic metamaterials also demonstrate a large number of novel phenomena resulting from the broadband singular behavior of their density of photonic states, which encompass enhanced quantum-electrodynamic effects, new stealth technology, thermal hyperconductivity [44–46], high Tc superconductivity [11,12], and very interesting gravitation theory analogues [3,13–17]. Moreover, hyperbolic metamaterial behavior appears to be compatible with photonic crystal effects, such as deep sub-wavelength light localization and giant field enhancement, resulting in a fascinating new class of artificial optical media – the photonic hypercrystals. Unique spectral properties of photonic hypercrystals lead to extreme sensitivity of the material to monolayer coatings of cobalt nanoparticles, which should find numerous applications in biological and chemical sensing.

References

[1] Podolskiy VA, Narimanov EE. Strongly anisotropic waveguide as a nonmagnetic left-handed system. Phys Rev B 2005;71:201101.
[2] Jacob Z, Alekseyev LV, Narimanov E. Optical hyperlens: far-field imaging beyond the diffraction limit. Opt Express 2006;14:8247–56.
[3] Smolyaninov II, Narimanov EE. Metric signature transitions in optical metamaterials. Phys Rev Lett 2010;105:067402.
[4] Smolyaninov II, Hung YJ, Davis CC. Magnifying superlens in the visible frequency range. Science 2007;315:1699–701.
[5] Liu Z, Lee H, Xiong Y, Sun C, Zhang X. Far-field optical hyperlens magnifying sub-diffraction-limited objects. Science 2007;315:1686.
[6] Jacob Z, Smolyaninov II, Narimanov EE. Broadband purcell effect: radiative decay engineering with metamaterials. Appl Phys Lett 2012;100:181105.
[7] Jacob Z, Kim J-Y, Naik GV, Boltasseva A, Narimanov EE, Shalaev VM. Engineering photonic density of states using metamaterials. App Phys B 2010;100:215.
[8] Noginov MA, Li H, Barnakov YuA, Dryden D, Nataraj G, Zhu G, et al. Controlling spontaneous emission with metamaterials. Opt Lett 2010;35: 1863.
[9] Narimanov E, Noginov MA, Li H, Barnakov Y. Darker than black: radiation-absorbing metamaterial. In: Quantum electronics and laser science conference, OSA Technical Digest (CD). Optical Society of America; 2010 [paper QPDA6].
[10] Narimanov EE, Smolyaninov II. Beyond Stefan-Boltzmann law: Thermal hyperconductivity arXiv:1109.5444.
[11] Smolyaninov II. Quantum topological transition in hyperbolic metamaterials based on high Tc superconductors. J Phys: Condens Matter 2014;26:305701.
[12] Smolyaninov II, Smolyaninova VN. Is there a metamaterial route to high temperature superconductivity? Adv Condens Matter Phys 2014;2014:479635.
[13] Smolyaninov II. Analogue gravity in hyperbolic metamaterials. Phys Rev A 2013;88:033843.
[14] Smolyaninov II, Yost B, Bates E, Smolyaninova VN. Experimental demonstration of metamaterial "multiverse" in a ferrofluid. Opt Exp 2013;21:14918–25.
[15] Smolyaninov II, Hung YJ. Modeling of time with metamaterials. JOSA B 2011;28:1591–5.
[16] Smolyaninov II, Hwang E, Narimanov EE. Hyperbolic metamaterial interfaces: hawking radiation from Rindler horizons and spacetime signature transtions. Phys Rev B 2012;85:235122.
[17] Smolyaninov II. Holographic duality in nonlinear hyperbolic metamaterials. J Optics 2014;16:075101.
[18] Narimanov EE, Kildishev AV. Metamaterials: naturally hyperbolic. Nat Photon 2015;9:214–6.
[19] Smolyaninov II. Vacuum in strong magnetic field as a hyperbolic metamaterial. Phys Rev Lett 2011;107:253903.
[20] Hoffman AJ, Alekseyev L, Howard SS, Franz KJ, Wasserman D, Podolskiy VA, et al. Negative refraction in semiconductor metamaterials. Nat Mater 2007;6:946.
[21] Noginov MA, Barnakov YuA, Zhu G, Tumkur T, Li H, Narimanov EE. Bulk photonic metamaterial with hyperbolic dispersion. Appl Phys Lett 2009;94:151105.
[22] Yao J, Liu Z, Liu Y, Wang Y, Sun C, Bartal G, et al. Optical negative refraction in bulk metamaterials. Science 2008;321:930.
[23] Wangberg R, Elser J, Narimanov EE, Podolskiy VA. Nonmagnetic nanocomposites for optical and infrared negative-refractive-index media. J Opt Soc Am B 2006;23:498–505.
[24] Jacob Z, Narimanov EE. Optical hyperspace for plasmons: Dyakonov states in metamaterials. Appl Phys Lett 2008;93:221109.
[25] Zayats AV, Smolyaninov II, Maradudin A. Nano-optics of surface plasmon-polaritons. Phys Rep 2005;408:131–314.
[26] Pohl DW, Courjon D, editors. Near field optics (NATO ASI-E Series). The Netherlands: Kluwer Academic Publishers; 1993.
[27] Smolyaninov II, Elliott J, Zayats AV, Davis CC. Far-field optical microscopy with nanometer-scale resolution based on the in-plane image magnification by surface plasmon polaritons. Phys Rev Lett 2005;94:057401.
[28] Lounis B, Orrit M. Single-photon sources. Rep Prog Phys 2005;68:1129.
[29] Morel Y, Smolyaninov II. Hyperbolic metamaterials as distributed Bragg mirrors for high power VCSEL devices. US Patent # 8,831,058.
[30] Smolyaninova VN, Yost B, Lahneman D, Narimanov E, Smolyaninov II. Self-assembled tunable photonic hyper-crystals. Sci Rep 2014;4:5706.
[31] Yablonovitch E. Inhibited spontaneous emission in solid-state physics and electronics. Phys Rev Lett 1987;58:2059–62.
[32] John S. Strong localization of photons in certain disordered dielectric superlattices. Phys Rev Lett 1987;58:2486–9.
[33] Pendry JB. Negative refraction makes a perfect lens. Phys Rev Lett 2000;85:3966–9.
[34] Krauss TF, DeLaRue RM, Brand S. Two-dimensional photonic-bandgap structures operating at near-infrared wavelengths. Nature 1996;383:699–702.
[35] Schurig D et al. Metamaterial electromagnetic cloak at microwave frequencies. Science 2006;314:977–80.
[36] Fleischmann M, Hendra PJ, McQuillan AJ. Raman spectra of pyridine adsorbed at a silver electrode. Chem Phys Lett 1974;26:163–6.
[37] Gao Y et al. Optical negative refraction in ferrofluids with magnetocontrollability. Phys Rev Lett 2010;104:034501.
[38] Zhang H, Widom M. Spontaneous magnetic order in strongly coupled ferrofluids. J Magn Magn Mater 1993;122:119–22.
[39] Lide DR, editor. CRC handbook of chemistry and physics. Boca Raton: CRC Press; 2005.
[40] Al-Ghouti MA, Al-Degs YS, Amer M. Determination of motor gasoline adulteration using FTIR spectroscopy and multivariate calibration. Talanta 2008;76:1105–12.
[41] Sun J, Shalaev MI, Litchinitser NM. Experimental demonstration of a nonresonant hyperlens in the visible spectral range. Nat Commun 2015;6:7201.
[42] Rho J, Ye Z, Xiong Y, Yin X, Liu Z, Choi H, et al. Spherical hyperlens for two-dimensional sub-diffractional imaging at visible frequencies. Nat Commun 2010;1:143.
[43] Iwanaga M. Hyperlens-array-implemented optical microscopy. Appl Phys Lett 2014;105:053112.
[44] Dyachenko PN, Molesky S, Petrov AYu, Störmer M, Krekeler T, Lang S, et al. Controlling thermal emission with refractory epsilon-near-zero metamaterials via topological transitions. Nat Commun 2016;7:11809.
[45] Guo Y, Jacob Z. Fluctuational electrodynamics of hyperbolic metamaterials. J Appl Phys 2014;115:234306.
[46] Guo Y, Jacob Z. Thermal hyperbolic metamaterials. Opt Exp 2013;21:15014–9.

Dr. Igor Smolyaninov is a Fellow of the Optical Society of America and a recipient of the Scientific American 50 Award. He graduated from the Moscow Institute of Physics and Technology in 1985 and received his PhD in 1990 from the Kapitza Institute for Physical Problems of the Russian Academy of Sciences. He has published more than 400 journal and conference papers and patents in various areas of surface optics, plasmonics, and electromagnetic metamaterials, and served as a principal investigator/technical lead on a number of NSF, CRDF and DARPA programs. He is a topical editor of JOSA B and a member of the editorial boards of Scientific Reports (Nature Publishing Group).

Dr. Vera Smolyaninova is a Professor of Physics in the Department of Physics, Astronomy and Geosciences at Towson University. She received her Ph.D. in physics from University of Maryland, College Park, 1999. She was awarded several NSF research grants including an NSF CAREER award. She worked extensively in the areas of electromagnetic metamaterials and transport, magnetic and thermal properties of functional oxides including superconductors. She is an expert in transformation optics, self-assembled three-dimensional hyperbolic metamaterials and metamaterial superconductors. She has published 70 papers in refereed journals and holds one patent. Her work in the area of metamaterials and transformation optics (invisibility cloaking, metamaterial superconductors, etc.) received wide press coverage in such outlets as BBC News, Physics World, EurekAlert! (AAAS), New Scientist, Scientific American, NSF news, EE times, and other general news media around the world.